

CryoFormer: Continuous Reconstruction of 3D Structures from Cryo-EM Data using Transformer-based Neural Representations

Xinhang Liu^{1,2,4†*}, Yan Zeng^{1,2*}, Yifan Qin^{1,2}, Hao Li^{1,2,3}, Jiakai Zhang^{1,2}, Lan Xu¹, Jingyi Yu¹
¹ShanghaiTech University ²Cellverse Technology ³iHuman Institute ⁴HKUST

Abstract

High-resolution heterogeneous reconstruction of 3D structures of proteins and other biomolecules using cryo-electron microscopy (cryo-EM) is essential for understanding fundamental processes of life. However, it is still challenging to reconstruct the continuous motions of 3D structures from hundreds of thousands of noisy and randomly oriented 2D cryo-EM images. Existing methods based on coordinate-based neural networks show compelling results to model continuous conformations of 3D structures in the Fourier domain, but they suffer from a limited ability to model local flexible regions and lack interpretability. We propose a novel approach, *cryoFormer*, that utilizes a transformer-based network architecture for continuous heterogeneous cryo-EM reconstruction. We for the first time directly reconstruct continuous conformations of 3D structures using an implicit feature volume in the 3D spatial domain. A novel deformation transformer decoder further improves reconstruction quality and, more importantly, locates and robustly tackles flexible 3D regions caused by conformations. In experiments, our method outperforms current approaches on three public datasets (1 synthetic and 2 experimental) and a new synthetic dataset of PEDV spike protein. The code and new synthetic dataset will be released for better reproducibility of our results. Project page: <https://cryoformer.github.io>.

1. Introduction

Dynamic objects as giant as planets and as minute as proteins constitute our physical world and produce nearly infinite possibilities of life forms. While computer vision has largely focused on modeling such object motions and shape variations at a macro scale, it is equally important to conduct a similar analysis on micro-scale proteins and other biomolecules, which helps reveal the fundamental

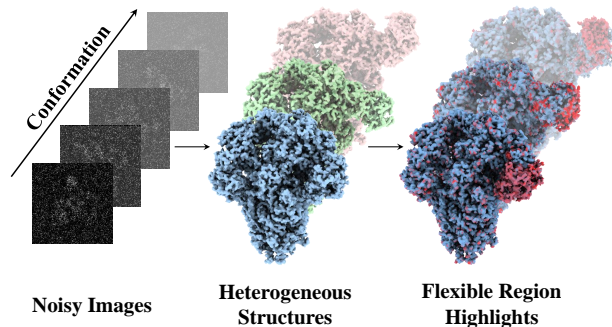


Figure 1. With noisy images as inputs, our method can successfully reconstruct the heterogeneous structures of proteins and highlight the local, flexible motions.

processes of biodynamics as well as facilitates drug development [19, 28, 35]. With recent advances in imaging techniques and data processing methods, cryo-electron microscopy (cryo-EM) can now capture hundreds of thousands of high-resolution images of biomolecules of random orientations under varying conformations. The collected dataset can be potentially used for recovering protein shapes and dynamics at an atom level via the single-particle analysis (SPA) technique.

The latest SPA solutions were unanimous extensions of existing shape recovery techniques designed to handle macro-scale objects. In reality, cryo-EM differs from classical imaging techniques in many ways. First, cryo-EM uses low electron dosage to minimize the damage to biological molecules, resulting in extremely noisy images. Further, the obtained protein images have unknown orientations that are difficult to calibrate due to a lack of features. Last, proteins exhibit conformational heterogeneity, i.e., the presence of continuous structural states of biological molecules. In particular, very few solutions can robustly recover multiple conformations of 3D structures in cryo-EM [40].

Existing software packages [38, 33] for high-resolution cryo-EM reconstruction typically adopt conventional approaches that may assume the 3D structure to be static or

† Work done while studying at ShanghaiTech University.

* Equal contribution.

can be classified into a discrete set of conformations, resulting in blurred and low-resolution results of flexible regions with continuous motions. Recently, there have been some neural approaches proposed for continuous heterogeneous cryo-EM reconstruction [51, 53, 22, 13, 32]. Similar to NeRF [26], cryoDRGN [51] uses an MLP to learn a continuous volumetric representation in the Fourier domain and additional latent space to model heterogeneity. cryoFIRE [22] adds a pose encoder for *ab-initio* heterogeneous reconstruction. However, such methods relying on Fourier domain heterogeneous reconstruction are hard to achieve high spatial resolution due to local continuous motions of flexible regions corresponding to a global discontinuous change in the Fourier domain. Flex3D [32] tends to improve the resolution of flexible regions by generating 3D deformation fields in the spatial domain. But it requires an additional 3D canonical map as input.

In this paper, we propose a novel approach, cryoFormer, that utilizes a transformer-based network architecture for continuous heterogeneous cryo-EM reconstruction. We, for the first time, directly reconstruct continuous conformations of 3D structures using an implicit feature volume in the 3D spatial domain to model local changes of conformations. A deformation transformer decoder further improves reconstruction quality and, more importantly, locates and robustly tackles flexible 3D regions caused by conformations, as illustrated in Fig. 1.

To efficiently model continuous changes of 3D local structures in the spatial domain, we first use an implicit spatial feature volume represented by hash encoding [27] augmented by a small MLP to reduce the computational costs while preserving geometric details significantly. Next, we deploy a pair of image encoders [51, 21] to extract the orientation feature and deformation feature, respectively. To generate the final density volume based on the extracted deformation and spatial features, we introduce a novel query-based deformation transformer decoder where both features are fused into structure queries. The queries, each corresponding to a specific part of the structure, first extract deformation information from an image by deformation-aware cross-attention and then integrate the spatial feature by spatial-wise cross-attention. Compared with directly using a pure MLP architecture to decode density, our transformer-based architecture is more effective and robust in fusing different modality information as well as visualizing flexible regions of 3D structures caused by varying conformations.

We validate cryoFormer on three public datasets (one synthetic and two experimental) and a new synthetic dataset of PEDV spike protein and achieve state-of-the-art reconstruction performance in terms of spatial resolution on both synthetic and real datasets, surpassing a number of baselines, including popular traditional softwares as well as neu-

ral approaches. Our method has the potential to address the limitations of traditional methods in reconstructing dynamic regions in biological structures, which often imply functional areas. We hope our approach can benefit the understanding of the mechanisms of molecular interactions.

2. Related Work

Conventional Cryo-EM Reconstruction. Traditional cryo-EM reconstruction involves the creation of a low-resolution model [20, 33] followed by the iterative refinement of the initial model [38, 33, 14]. Standard approaches for addressing structural heterogeneity [37, 25] involve discretization of dynamics and are not able to continuously reconstruct the motion process. Most algorithms perform reconstruction in the Fourier domain since it allows for efficient computation of the forward-projection and back-projection operations. Some approaches are based on reconstruction in the spatial domain and using a flow field to model the structural motion [32, 8]. Our approach also conveys reconstruction in the spatial domain, while instead of utilizing a flow field to model, we propose a query-based transformer architecture to tackle conformational heterogeneity.

Neural Representations for Cryo-EM Reconstruction. Neural representations learn to encode a coordinate-to-value mapping for 3D shape modeling. Instead of storing the discrete signal values in a grid, neural representations model discrete data as samples of a continuous manifold using multi-layer perceptions (MLP). They have notably contributed to novel view synthesis [26, 2], geometry [45, 29, 49] and dynamic scene modeling [31, 48, 30].

Efforts have been made to use neural representations for volume reconstruction in cryo-EM. CryoDRGN [51, 52] first proposed using a Multi-Layer Perceptron (MLP) with positional encoding to represent biological structures. This usage of neural representation allows for the continuous modeling of deformations, leading to excellent results in accounting for the molecule’s continuous changes. Following this success, cryoDRGN-like architectures were utilized to develop reconstruction approaches without the need for pre-computed poses, also known as *ab-initio* reconstruction [53, 21, 22]. Sparse Fourier Backpropagation [18] proposed to express the cryoDRGN-like VAE reconstruction on a volumetric grid and lower computational cost. ResMFN [39] proposes a coordinate network architecture that enables coarse-to-fine optimization with fine-grained control over the frequency support of learned reconstructions to deal with cryo-EM reconstruction where coarse-to-fine estimation is required. Different from previous work building neural representations in the Fourier domain for cryo-EM reconstruction, our approach directly reconstructs continuous conformations of 3D structures using an implicit feature volume in the 3D spatial domain to model local

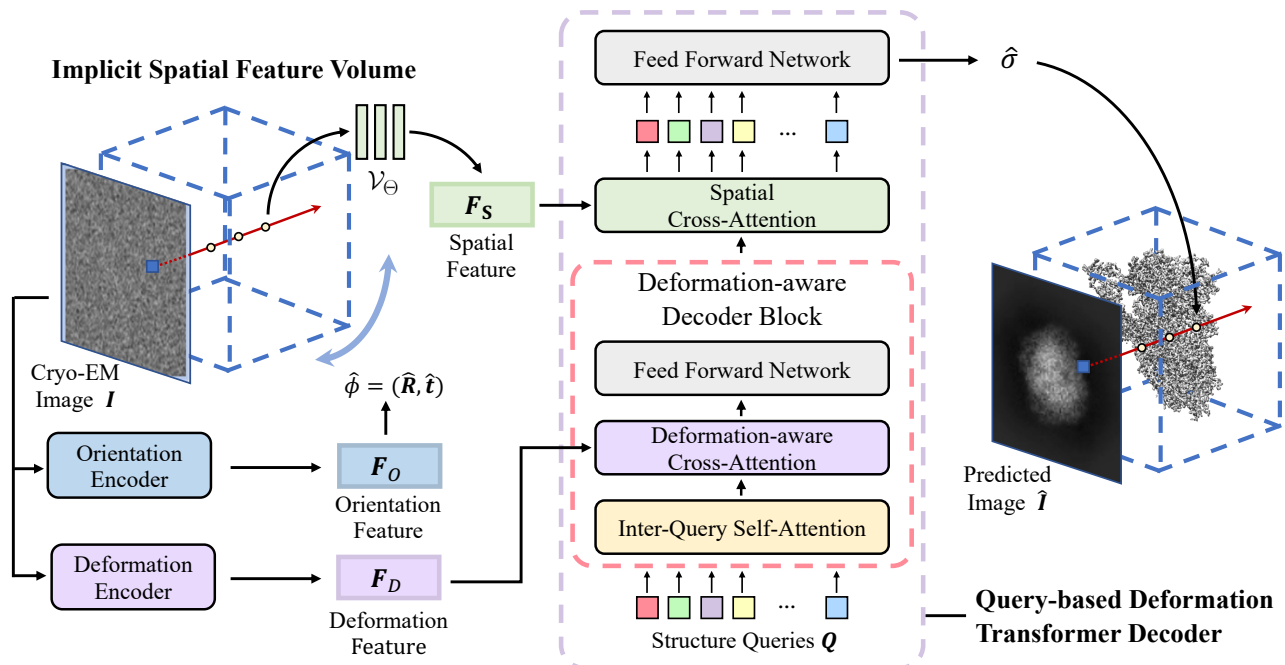


Figure 2. **Pipeline of cryoFormer**. **1)** An input image is fed into image encoders that output the orientation feature and the deformation feature. **2)** Rotated coordinates are fed into our implicit neural spatial feature volume to produce a spatial feature. **3)** The spatial feature and the deformation image feature interact in the deformation transformer decoder to output the density prediction.

changes of conformations.

Transformers. Transformers have become a ubiquitous learning architecture capable of capturing long-range dependencies in sequential data, and have demonstrated remarkable success across a range of applications, including natural language processing [43, 10, 4], computer vision [11, 23], and protein structure determination [17]. Various downstream tasks in computer vision have adopted Transformer-based models, including image classification [11], object detection [5], semantic/instance segmentation [6, 41, 47, 50], video understanding [54, 1, 24, 7]. Transformers also benefit neural representations in training with sparse input views and generalization across scenes [46, 34, 44]. In this work, we incorporate a transformer decoder where structure queries interact with the deformation and spatial features to predict the potential field.

3. Method

3.1. Image Formation Model

In the cryo-EM image formation model, the 3D biological structure is represented as a function $\sigma : \mathbb{R}^3 \mapsto \mathbb{R}^+$, which expresses the Coulomb potential induced by the atoms. To recover the potential function, the probing electron beam interacts with the electrostatic potential and results in projections $\{\mathbf{I}_i\}_{1 \leq i \leq n}$. Specifically, each projection

can be expressed as

$$\mathbf{I}(x, y) = g \star \int_{\mathbb{R}} \sigma(\mathbf{R}^\top \mathbf{x} + \mathbf{t}) dz + \epsilon, \quad \mathbf{x} = (x, y, z)^\top \quad (1)$$

where $\mathbf{R} \in SO(3)$ is an orientation representing the 3D rotation of the molecule and $\mathbf{t} = (t_x, t_y, 0)^\top$ is an in-plane translation corresponding to an offset between the center of projected particles and center of the image. The projection is, by convention, assumed to be along the z -direction after rotation. The image signal is convolved with g , a pre-estimated point spread function (PSF) for the microscope, before being corrupted with the noise ϵ and registered on a discrete grid of size $D \times D$, where D is the size of the image along one dimension. A more detailed formulation for cryo-EM reconstruction is given in Appendix.

3.2. Overview of CryoFormer

We propose a novel approach, cryoFormer, that uses an implicit spatial feature volume as well as transformer-based network architecture for continuous heterogeneous cryo-EM reconstruction. Fig. 2 demonstrates the pipeline of cryoFormer. To extract conformation and pose information of an image, an input projection image \mathbf{I} is fed into image encoders that output an orientation feature F_O and a deformation feature F_D . F_O is then converted to a pose $\hat{\phi} = (\hat{\mathbf{R}}, \hat{\mathbf{t}})$,

though it can be skipped if an accurate estimated pose is pre-computed. $\hat{\mathbf{R}}$ is an rotation matrix to rotate a grid with size D^3 in the spatial domain.

The rotated coordinates are then fed into our implicit neural spatial feature volume, \mathcal{V}_Θ , parameterized by Θ . \mathcal{V}_Θ is a mapping from coordinates in \mathbb{R}^3 to spatial features in $\mathbb{R}^{N \times C}$ that contains spatial-related structural information as well as learned conformational information. We sample each 3D point in a rotated 3D grid, and implicit neural spatial feature volume outputs a spatial feature F_S . Then we feed F_S into the deformation transformer decoder, where it interacts with structure queries Q and the deformation image feature F_D to output the density prediction σ . This transformer-based architecture design improves the reconstruction performance and enables the highlighting of 3D flexible regions of results.

3.3. Implicit Spatial Feature Volume

To reduce the storage consumption while modeling continuous conformations of 3D structures, neural representation encodes the scene as a continuous high-dimensional manifold and has shown its huge potential in cryo-EM heterogeneous reconstruction tasks [51, 52, 53, 21, 22]. We, for the first time, directly reconstruct continuous conformations of 3D structures using an implicit feature volume, denoted $\mathcal{V}_\Theta(x, y, z; \Theta)$ in the 3D spatial domain to model local changes of conformations. Inspired by Instant NGP [27] for efficient 3D representation training and rendering, we use a similar multi-resolution hash grid encoding augmented by a single-layer MLP to decode a high-dimensional spatial feature $F_S \in \mathbb{R}^{N \times C}$, which preserve the high-frequency details with highly reduced computational cost compared with a NeRF-like global coordinate-based MLP in other cryo-EM work [51, 21, 22]

$$\mathcal{V}_\Theta(x, y, z; \Theta) = F_S \quad (2)$$

Compared to other methods that reconstruct structures in Fourier domain [51, 53, 21, 22], reconstruction in the spatial domain [32] is more explainable, easier to model local changes of flexible regions and redeems the artifacts from the sparse sampling rate of high frequency in Fourier domain.

3.4. Orientation and Deformation Image Encoders

Since the underlying particle’s relative pose and conformational state for each given cryo-EM image may be unknown, we use two image encoders to extract orientation features and deformation features respectively. For both encoders, we adopt MLPs containing 10 hidden layers of width 128 with ReLU activations, following the image encoder design of cryoDRGN [51, 52].

Orientation Encoder. For each image, the orientation encoder estimates a biological structure’s relative pose, which

includes rotation and translation, i.e., $\hat{\phi} = (\hat{\mathbf{R}}, \hat{\mathbf{t}})$. The rotation is first represented in a 6-dimensional space, denoted as $\mathbb{S}^2 \times \mathbb{S}^2$ [55] and then converted to the matrix format. The orientation encoder is designed for *ab-initio* prediction or refinement of pose and can be removed when an accurate pose is pre-computed for each image.

Deformation Encoder. The deformation encoder maps a projection into a deformation feature representation $F_D \in \mathbb{R}^{N \times C}$. F_D will interact with spatial features in the query-based deformation transformer decoder to output the density estimation $\hat{\sigma}$. Therefore, $\hat{\sigma}$ is conditioned on F_D .

3.5. Query-based Deformation Transformer Decoder

To generate the final density volume based on the extracted deformation and spatial features, we introduce a novel query-based deformation transformer decoder where both features are fused into queries, to map to a specific part of the structure. Spatial features from the implicit feature volume are fed into the query-based deformation transformer decoder, where they interact with the image deformation feature to generate the final estimated density value $\hat{\sigma}$. The transformer decoder uses a cross-attention mechanism to fuse information from different sources or modalities. We use Attention to denote the scaled dot-product attention, which operates as

$$\text{Attention}(Q, K, V) = \text{softmax}\left(\frac{QK^T}{\sqrt{C}}\right)V, \quad (3)$$

where $Q, K, V \in \mathbb{R}^{N \times C}$ are called the query, key, and value matrices; N and C indicate the token number and the hidden dimension. When $Q = K = V$, we call such operation “self-attention”.

Structure Query Prototypes. We denote randomly-initialized learnable structure queries as $Q \in \mathbb{R}^{N \times C}$. Ideally, each of the N structure queries corresponds to some component of the reconstructed structure. Every component has its own conformational heterogeneity leading to different behavior (or density distribution) in the space.

Deformation-aware Decoder Block. Given an image with its deformation feature F_D , the structure queries first interact with F_C in the deformation-aware decoder blocks. Each query captures information about the behavior of its corresponding component in the input image. Each deformation-aware block sequentially consists of an inter-query self-attention block, a deformation-aware cross-attention layer, and a feed-forward network (FFN), where the deformation-aware cross-attention layer is computed as $\text{Attention}(Q, F_D, Q)$. We stack three decoder blocks for fusing deformation cues into structure queries.

Spatial Density Estimation. To estimate the density value at a specific coordinate, the queries then interact with its spatial feature F_S by spatial cross attention:

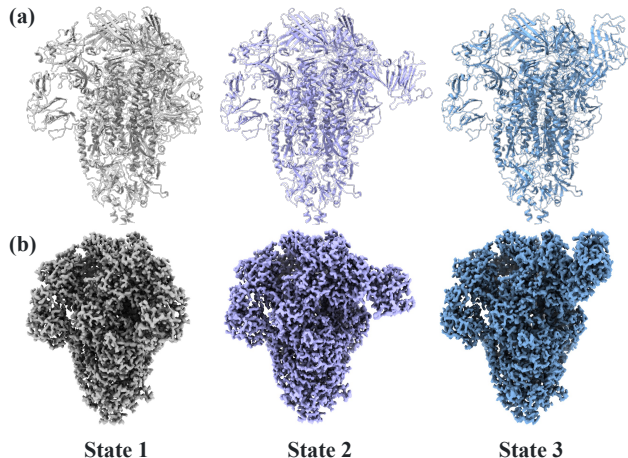


Figure 3. **Visualization of PEDV spike protein dataset.** (a) Our manually modified atomic models (PDB files) in the intermediate states. (b) Their corresponding converted density fields (MRC files).

Attention(Q, F_C, Q). In this operation, each query captures its underlying component’s behavior (determined by the image deformation feature) at the arbitrary 3D position, directly manifested as the density value. Finally, an FFN maps the queries to the estimated density $\hat{\sigma}$.

3.6. Training Scheme

To train our comprehensive system, we first calculate the projected pixel value of the predicted image from the estimated density volume corresponding to the input image (Eqn. 4), which is the output of a query-based deformation transformer decoder.

$$\hat{\mathbf{I}}(x, y) = \hat{g} \star \int_{\mathbb{R}} \hat{\sigma}(\hat{\mathbf{R}}^\top \mathbf{x} + \hat{\mathbf{t}}) dz + \epsilon, \quad \mathbf{x} = (x, y, z)^\top \quad (4)$$

where \hat{g} is the point spread function (PSF) of the projected image, assumed to be known from contrast transfer function (CTF) correction [36] in the image pre-processing stage.

The loss function is to measure the squared error between the observed images $\{\mathbf{I}_i\}_{1 \leq i \leq n}$ and the predicted images $\{\hat{\mathbf{I}}_i\}_{1 \leq i \leq n}$ by Eqn. 4,

$$\mathcal{L} = \sum_{i=1}^n \left\| \mathbf{I}_i - \hat{\mathbf{I}}_i \right\|_2^2 \quad (5)$$

Unlike the squared loss function derived from the central slice theorem in the Fourier domain, as a spatial domain reconstruction approach, our loss term involves the multi-view constraints from orthogonal spatial projections of a 3D volume.

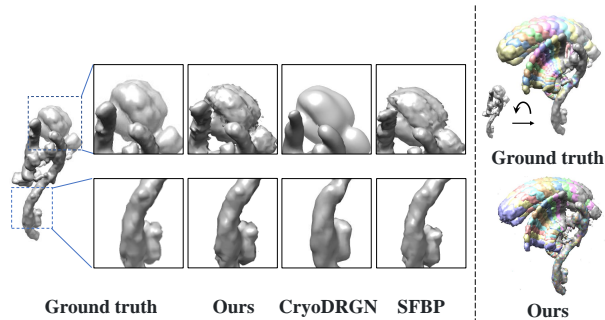


Figure 4. **Qualitative comparison of different methods on cryoDRGN Synthetic Dataset.** cryoFormer reconstructed volumes qualitatively match the ground truth and baselines’ reconstructed structures, with better recovery of details. As shown in the right, cryoFormer is capable of continuously modeling the conformational heterogeneity.

4. PEDV Spike Protein Dataset

To better evaluate algorithms for heterogeneous cryo-EM reconstruction, we create a synthetic dataset based on the spike protein of the porcine epidemic diarrhea virus (PEDV). The spike protein is a homotrimer, with each monomer containing a domain 0 (D0) region that modulates the enteric tropism of PEDV by binding to sialic acids (SAs) on the surface of enterocytes [15] and can exist in both “up” and “down” states. [16] determined the atomic coordinates of PEDV PT52 S and deposited them in the Protein Data Bank (PDB) [3] under the accession codes 7W6M and 7W73 .

We utilized Pymol software [9] to manually supplement the reasonable process of the movement of the D0 region in the format of intermediate atomic models (Fig. 3 (a)). We converted these atomic models (PDB files) to discrete potential maps (MRC files) using *pdb2mrc* module from EMAN2 software [42], which were then projected into 2D images (Fig. 3 (b)). We then simulate the image formation model as in Eqn. 1 at 20k rotations uniformly sampled on $SO(3)$. We model ϵ as zero-mean white Gaussian noise and apply the PSF. We adjust the noise scale to produce the required SNR. We will make the atomic models, density maps, and simulated projections publicly available with the aim of advancing cryo-EM reconstruction algorithms.

5. Results

In this section, we present qualitative and quantitative evaluations of cryoFormer for heterogeneous cryo-EM reconstruction. We verify cryoFormer on two synthetic datasets by modeling conformational heterogeneity and recovering structural details. Next, we evaluate cryoFormer

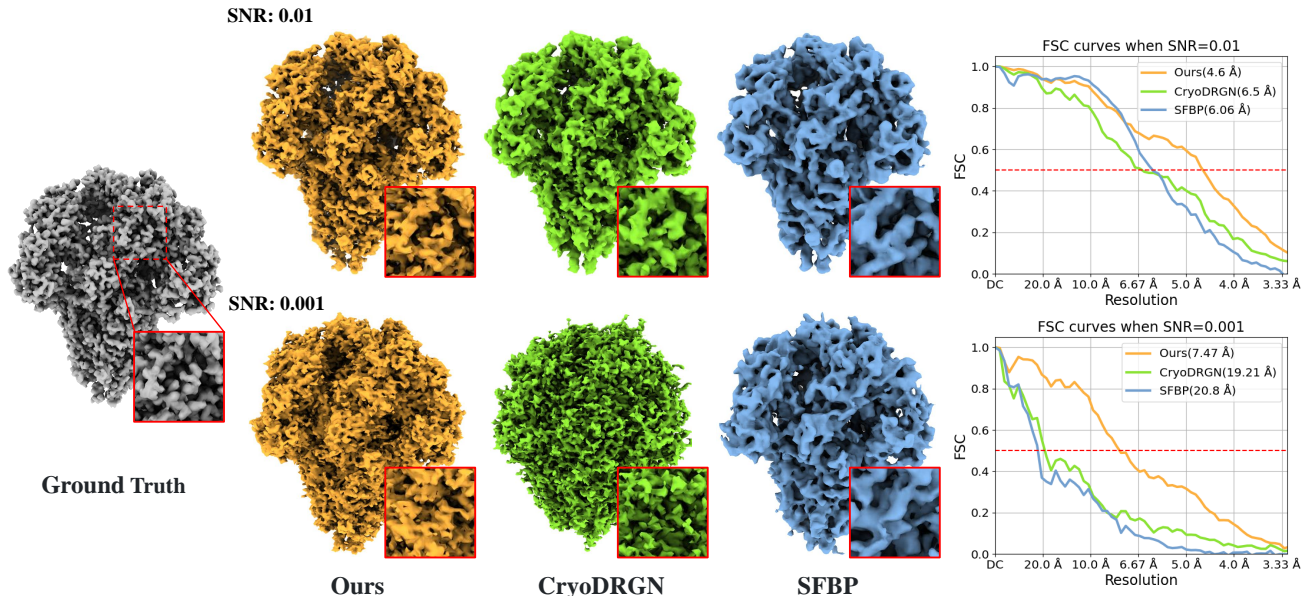


Figure 5. **Qualitative and quantitative comparison of different methods on PEDV spike dataset.** We compare cryoFormer with cryoDRGN and SFBP on PEDV spike dataset, with $\text{SNR} = 0.01$ and $\text{SNR} = 0.001$. **Left:** Reconstructed 3D volumes. Under different levels of the noise intensity, the volumes reconstructed by cryoFormer exhibit better restoration of details than the baseline. **Right:** The average FSC to each ground truth of for cryoFormer, cryoDRGN, and SFBP, where a higher curve indicates better reconstruction.

on a real experimental dataset with minimal structural motions. We then evaluate cryoFormer on a real experimental dataset with significant conformational heterogeneity to test cryoFormer’s capability for heterogeneous reconstruction in real data.

We use ground-truth poses for synthetic datasets, and pre-computed poses for real experimental datasets, so we skip the orientation encoder from our architecture for better expositions.

Implementation details. For the implicit spatial feature volume, we utilized a hash grid with 16 levels, where the number of features in each level is 2, the hashmap size is 2^{15} , and the base resolution is 16. This hash grid is followed by a tiny MLP with one layer and hidden dimension 16. The choice of the query-based deformation transformer’s parameters is discussed in Sec. 5.4. We trained our model on a single NVIDIA GeForce RTX 3090 Ti GPU. The training time depends on the number of images and their resolution in the dataset. It takes approximately 4 hours to train our method for a real dataset of around 100,000 images with a resolution of 128.

We provide additional experimental details and results in the supplementary materials, including video results, and encourage readers to refer to them.

5.1. Heterogeneous Reconstruction on Synthetic Datasets

We first evaluate cryoFormer on two synthetic datasets: 1) the synthetic dataset proposed by [51], generated from an atomic model of a protein complex, and 2) our proposed PEDV spike dataset.

We compare cryoFormer against cryoDRGN [51] and Sparse Fourier Backpropagation (SFBP) [18] as representatives of VAE-based methods.

CryoDRGN Synthetic Dataset. This dataset contains 50k image with size $D = 64$ and $\text{SNR} = 0.1$ from an atomic model of a protein complex containing a 1D continuous motion [51].

In Fig. 4, we show that cryoFormer reconstructed volumes qualitatively match the ground truth and baselines’ reconstructed structures. Note that while we only visualize 10 structures sampled along the latent space, we can reconstruct the full continuum of states. CryoDRGN and SFBP also succeeded in continuously modeling the conformational heterogeneity but retaining fewer details than ours.

PEDV Spike Protein Dataset. We use our proposed PEDV spike dataset containing 20k image with size $D = 128$. To test the performance of the algorithm under different levels of noise scale, we conducted experiments in two settings: $\text{SNR} = 0.01$ and $\text{SNR} = 0.001$. We also compare the results with the ground truth as it is a synthetic dataset.

As is shown in Fig. 5 left, our method produces bet-

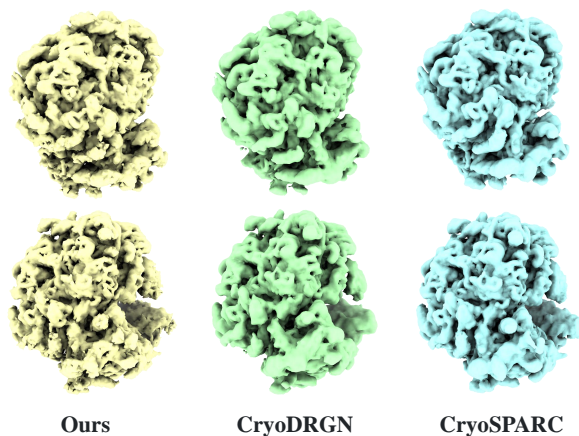


Figure 6. **Qualitative comparison for homogeneous cryo-EM reconstruction on EMPIAR-10028.** Our method matches or even outperforms baselines in terms of reconstructing fine details of biological structures. The two rows show the same reconstructed structure viewed from different angles.

ter reconstruction than cryoDRGN and SFBP, with better-recovered details under different levels of the noise scale. Here we only present one state of heterogeneous reconstruction, and we leave out the presentation of others in the supplementary material.

We measured the Fourier shell correlation (FSC) between the reconstructed and the ground truth structures. As is done in [18], the FSC is measured as the normalized correlation between Fourier components of the solvent-masked reconstruction and the known ground truth for each frequency band, averaged over 30 samples (three out of each conformation). In Fig. 5 right, we show the FSC curves of our method, cryoDRGN, and SFBP. A higher curve indicates better performance. Under different levels of noise intensity, our quantitative results outperform all other baselines. Particularly at $\text{SNR} = 0.001$, the metrics of the baselines decrease significantly because of the failure to restore high-frequency information.

5.2. Homogeneous Reconstruction on Experimental Datasets

Next, we present our experimental results of cryoFormer on real experimental datasets. We begin by testing cryoFormer on a dataset with ignorable biological motion, using it for homogeneous reconstruction. It is worth noting that although cryoFormer is designed for the more challenging task of heterogeneous reconstruction, we retain the architecture of cryoFormer without modification for homogeneous reconstruction. We use the real dataset from EMPIAR-10028, which consists of 105,247 images of the 80S ribosome downsampled to an image size of 128. Here we perform homogeneous reconstruction with cryo-

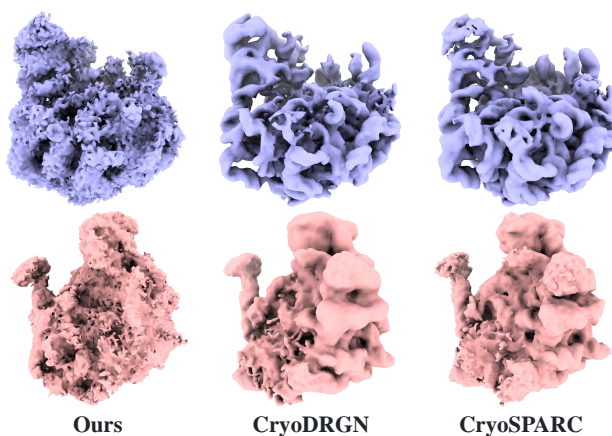


Figure 7. **Qualitative comparison for heterogeneous cryo-EM reconstruction on EMPIAR-10076.** Our method outperforms cryoDRGN and cryoSPARC in terms of the quality of heterogeneous reconstruction and is able to model the dynamic structures with finer details.

DRGN [51], a representative neural representation-based method, and cryoSPARC [33], a traditional state-of-the-art method.

As is shown in Fig. 6, reconstructed volumes from our method match or even surpass those from baseline methods, especially in certain details. Since this is real data without available ground truth to quantitatively evaluate performance, we follow typical practice by splitting the full dataset into two halves, reconstructing each half separately, and computing the FSC between them. We included the FSC curves of this experiment in the appendix.

5.3. Heterogeneous Reconstruction on Experimental Datasets

To test cryoFormer’s capability of heterogeneous reconstruction, we evaluate it on a real experimental dataset containing significant heterogeneity. We use the real dataset from EMPIAR-10076, which consists of 131,899 images of the *E. coli* large ribosomal subunit (LSU) undergoing assembly.

We perform heterogeneous reconstruction using cryoFormer, cryoDRGN [51] and cryoSPARC [33] (using multiclass refinement). As shown in Fig. 7, when processing data containing multiple conformational states, both cryoDRGN and cryoSPARC can only reconstruct the outline of the structure without retaining finer details. In contrast, our method can successfully model the heterogeneity of the data while keeping fine details.

5.4. Evaluation

To validate our architectural designs, we conduct the following evaluations on the PEDV spike dataset. We use a

Method	best	second-best
	Resolution (\downarrow)	Time (\downarrow)
positional encoding	6.18	8.3h
Fourier domain	9.99	2.11h
w/o transformer	8.9	0.91h
Ours ($N = 32, C = 32$)	5.34	1.4h
Ours ($N = 64, C = 32$)	4.83	1.33h
Ours ($N = 32, C = 64$)	4.93	1.21h
Ours ($N = 64, C = 64$)	4.74	1.39h

Table 1. **Quantitative evaluation on our design choices.** We evaluate the core design of our implicit spatial feature volume and deformation transformer decoder. When $N = 64, C = 64$, our full model in the spatial domain achieves the highest performance of spatial resolution with little sacrifice of training speed.

dataset with 20,000 projections with $\text{SNR} = 0.01$. In all experiments, we run variants of cryoFormer for 100 epochs to guarantee convergence. We quantify the accuracy of the reconstructed volume by computing the FSC between the reconstruction and the ground truth and reporting the resolution at the 0.5 cutoff in \AA .

Implicit spatial feature volume. Different from recent cryo-EM reconstruction using Fourier domain neural representations [51, 53, 21, 22], cryoFormer uses a spatial feature volume built in the spatial domain with hash grid [27]. We evaluate two variants of cryoFormer with changed neural representation. In Tab. 1, “positional encoding” stands for using positional encoding with a large global MLP, and “Fourier domain” stands for building the hash grid neural representation in the Fourier domain. Both variants show significantly decreased reconstruction resolution and increased time consumption.

Deformation Transformer. We design the query-based deformation transformer decoder to bring about the interaction between the deformation features and the coordinate features. We evaluate a variant of cryoFormer, where coordinate features and image deformation features are directly concatenated and fed into a single MLP to output a density value. As in Tab. 1 “w/o transformer”, it is more time-efficient but achieves worse reconstruction ability than ours. We also change the parameter of our deformation transformer decoder and report their reconstruction resolution and time. We take $N = 64, C = 64$ as our default setting.

Interpretation on the 3D attention maps. 3D attention maps are computed at each coordinate by spatial cross-attention between its spatial feature and deformation-aware queries. The value is used as the surface color of the reconstructed volume. We manually set a threshold, the regions above it are colored in red, and the rest are colored in blue. As is shown in Fig. 8, the displayed channel of attention map captures information about the regions of the PEDV spike that exhibit noticeable motion.

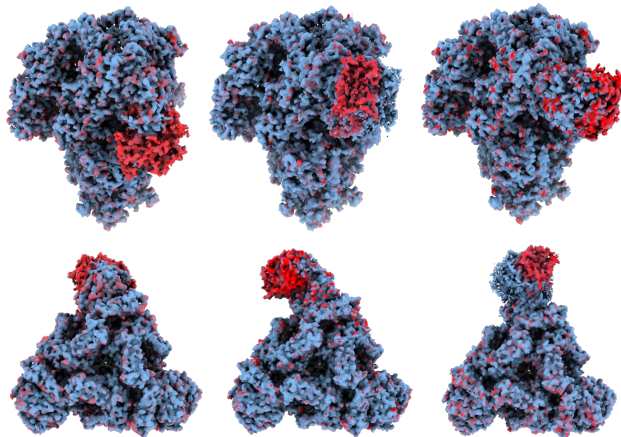


Figure 8. **Visualization of 3D attention map.** We map the value in the attention map to the surface color of the reconstructed volume. The displayed channel of the 3D attention map captures information about the flexible regions of the PEDV spike. The top and bottom rows show the same attention map viewed from different angles.

6. Discussion

Limitations. As the first trial to tackle continuous heterogeneous reconstruction of cryo-EM structures in the spatial domain, our approach suffers from some limitations. Though we use hash encoding for efficient training and inferring, our method still demands a significant amount of computational resources and requires a lengthy training process that prevents us from processing raw full-resolution images of cryo-EM data. Also, our pose module [21, 22] cannot fully handle *ab-initio* reconstruction without pre-computed poses. To support it, developing an improved pose module may indicate a future research direction.

Conclusion. We have presented cryoFormer, the first approach that uses a transformer-based network for continuous heterogeneous cryo-EM reconstruction in the spatial domain. For efficient training and inference, we use hash encoding augmented by a small MLP to reconstruct a feature volume in the spatial domain. Our novel deformation-aware transformer decoder combines conformation features and spatial features to generate the final spatial density volume. Finally, Our transformer-based architecture supports a new capability of highlighting flexible regions of 3D structures. The experimental results show that our method outperforms other methods in both synthetic and real datasets. Our approach holds great promise to better understand the fundamental processes of life by revealing the unseen conformations of 3D biomolecules.

References

- [1] Anurag Arnab, Mostafa Dehghani, Georg Heigold, Chen Sun, Mario Lučić, and Cordelia Schmid. Vivit: A video vision transformer. In *IEEE/CVF International Conference on Computer Vision (ICCV)*, pages 6836–6846, 2021. [3](#)
- [2] Jonathan T Barron, Ben Mildenhall, Matthew Tancik, Peter Hedman, Ricardo Martin-Brualla, and Pratul P Srinivasan. Mip-nerf: A multiscale representation for anti-aliasing neural radiance fields. In *IEEE/CVF Conference on Computer Vision and Pattern Recognition (CVPR)*, pages 5855–5864, 2021. [2](#)
- [3] Helen M Berman, John Westbrook, Zukang Feng, Gary Gilliland, Talapady N Bhat, Helge Weissig, Ilya N Shindyalov, and Philip E Bourne. The protein data bank. *Nucleic acids research*, 28(1):235–242, 2000. [5](#)
- [4] Tom Brown, Benjamin Mann, Nick Ryder, Melanie Subbiah, Jared D Kaplan, Prafulla Dhariwal, Arvind Neelakantan, Pranav Shyam, Girish Sastry, Amanda Askell, et al. Language models are few-shot learners. *Advances in Neural Information Processing Systems (NeurIPS)*, 33:1877–1901, 2020. [3](#)
- [5] Nicolas Carion, Francisco Massa, Gabriel Synnaeve, Nicolas Usunier, Alexander Kirillov, and Sergey Zagoruyko. End-to-end object detection with transformers. In *European Conference on Computer Vision (ECCV)*, pages 213–229. Springer, 2020. [3](#)
- [6] Hanting Chen, Yunhe Wang, Tianyu Guo, Chang Xu, Yiping Deng, Zhenhua Liu, Siwei Ma, Chunjing Xu, Chao Xu, and Wen Gao. Pre-trained image processing transformer. In *IEEE/CVF Conference on Computer Vision and Pattern Recognition (CVPR)*, pages 12299–12310, 2021. [3](#)
- [7] Jiaben Chen, Renrui Zhang, Dongze Lian, Jiaqi Yang, Ziyao Zeng, and Jianbo Shi. iquery: Instruments as queries for audio-visual sound separation. *IEEE/CVF Conference on Computer Vision and Pattern Recognition (CVPR)*, 2023. [3](#)
- [8] Muyuan Chen and Steven J Ludtke. Deep learning-based mixed-dimensional gaussian mixture model for characterizing variability in cryo-em. *Nature methods*, 18(8):930–936, 2021. [2](#)
- [9] Warren L DeLano et al. Pymol: An open-source molecular graphics tool. *CCP4 Newsl. Protein Crystallogr*, 40(1):82–92, 2002. [5](#)
- [10] Jacob Devlin, Ming-Wei Chang, Kenton Lee, and Kristina Toutanova. Bert: Pre-training of deep bidirectional transformers for language understanding. *arXiv preprint arXiv:1810.04805*, 2018. [3](#)
- [11] Alexey Dosovitskiy, Lucas Beyer, Alexander Kolesnikov, Dirk Weissenborn, Xiaohua Zhai, Thomas Unterthiner, Mostafa Dehghani, Matthias Minderer, Georg Heigold, Sylvain Gelly, et al. An image is worth 16x16 words: Transformers for image recognition at scale. *International Conference on Learning Representations (ICLR)*, 2020. [3](#)
- [12] Thomas D Goddard, Conrad C Huang, Elaine C Meng, Eric F Pettersen, Gregory S Couch, John H Morris, and Thomas E Ferrin. Ucsf chimerax: Meeting modern challenges in visualization and analysis. *Protein Science*, 27(1):14–25, 2018. [12](#)
- [13] Harshit Gupta, Thong H Phan, Jaejun Yoo, and Michael Unser. Multi-cryogan: Reconstruction of continuous conformations in cryo-em using generative adversarial networks. In *Computer Vision—ECCV 2020 Workshops: Glasgow, UK, August 23–28, 2020, Proceedings, Part I 16*, pages 429–444. Springer, 2020. [2](#)
- [14] Michael Hohn, Grant Tang, Grant Goodyear, Philip R Baldwin, Zhong Huang, Pawel A Penczek, Chao Yang, Robert M Glaeser, Paul D Adams, and Steven J Ludtke. Sparx, a new environment for cryo-em image processing. *Journal of structural biology*, 157(1):47–55, 2007. [2](#)
- [15] Yixuan Hou, Chun-Ming Lin, Masaru Yokoyama, Boyd L Yount, Douglas Marthaler, Arianna L Douglas, Shristi Ghimire, Yibin Qin, Ralph S Baric, Linda J Saif, et al. Deletion of a 197-amino-acid region in the n-terminal domain of spike protein attenuates porcine epidemic diarrhea virus in piglets. *Journal of virology*, 91(14):e00227–17, 2017. [5](#)
- [16] Cheng-Yu Huang, Piotr Draczkowski, Yong-Sheng Wang, Chia-Yu Chang, Yu-Chun Chien, Yun-Han Cheng, Yi-Min Wu, Chun-Hsiung Wang, Yuan-Chih Chang, Yen-Chen Chang, et al. In situ structure and dynamics of an alpha-coronavirus spike protein by cryo-et and cryo-em. *Nature communications*, 13(1):4877, 2022. [5](#)
- [17] John Jumper, Richard Evans, Alexander Pritzel, Tim Green, Michael Figurnov, Olaf Ronneberger, Kathryn Tunyasuvunakool, Russ Bates, Augustin Židek, Anna Potapenko, et al. Highly accurate protein structure prediction with alphafold. *Nature*, 596(7873):583–589, 2021. [3](#)
- [18] Dari Kimanius, Kiarash Jamali, and Sjors HW Scheres. Sparse fourier backpropagation in cryo-em reconstruction. In *Advances in Neural Information Processing Systems (NeurIPS)*, 2022. [2](#), [6](#), [7](#), [12](#)
- [19] Werner Kühlbrandt. The resolution revolution. *Science*, 343(6178):1443–1444, 2014. [1](#), [12](#)
- [20] Andres E Leschziner and Eva Nogales. The orthogonal tilt reconstruction method: an approach to generating single-class volumes with no missing cone for ab initio reconstruction of asymmetric particles. *Journal of structural biology*, 153(3):284–299, 2006. [2](#)
- [21] Axel Levy, Frédéric Poitevin, Julien Martel, Youssef Nashed, Ariana Peck, Nina Miolane, Daniel Ratner, Mike Dunne, and Gordon Wetzstein. CryoAI: Amortized inference of poses for ab initio reconstruction of 3D molecular volumes from real cryo-EM images. In *IEEE/CVF Conference on Computer Vision and Pattern Recognition (CVPR)*, 2022. [2](#), [4](#), [8](#), [14](#)
- [22] Axel Levy, Gordon Wetzstein, Julien Martel, Frederic Poitevin, and Ellen D Zhong. Amortized inference for heterogeneous reconstruction in cryo-em. *Advances in Neural Information Processing Systems (NeurIPS)*, 2022. [2](#), [4](#), [8](#), [14](#)
- [23] Ze Liu, Yutong Lin, Yue Cao, Han Hu, Yixuan Wei, Zheng Zhang, Stephen Lin, and Baining Guo. Swin transformer: Hierarchical vision transformer using shifted windows. In *IEEE/CVF International Conference on Computer Vision (ICCV)*, pages 10012–10022, 2021. [3](#)
- [24] Ze Liu, Jia Ning, Yue Cao, Yixuan Wei, Zheng Zhang, Stephen Lin, and Han Hu. Video swin transformer. In

- IEEE/CVF Conference on Computer Vision and Pattern Recognition (CVPR)*, pages 3202–3211, 2022. 3
- [25] Dmitry Lyumkis, Axel F Brilot, Douglas L Theobald, and Nikolaus Grigorieff. Likelihood-based classification of cryo-em images using frealign. *Journal of structural biology*, 183(3):377–388, 2013. 2
- [26] Ben Mildenhall, Pratul P. Srinivasan, Matthew Tancik, Jonathan T. Barron, Ravi Ramamoorthi, and Ren Ng. Nerf: Representing scenes as neural radiance fields for view synthesis. In *European Conference on Computer Vision (ECCV)*, 2020. 2
- [27] Thomas Müller, Alex Evans, Christoph Schied, and Alexander Keller. Instant neural graphics primitives with a multiresolution hash encoding. *ACM Transactions on Graphics (TOG)*, 41(4):102:1–102:15, July 2022. 2, 4, 8
- [28] Eva Nogales. The development of cryo-em into a mainstream structural biology technique. *Nature methods*, 13(1):24–27, 2016. 1, 12
- [29] Michael Oechsle, Songyou Peng, and Andreas Geiger. Unisurf: Unifying neural implicit surfaces and radiance fields for multi-view reconstruction. In *IEEE/CVF Conference on Computer Vision and Pattern Recognition (CVPR)*, pages 5589–5599, 2021. 2
- [30] Keunhong Park, Utkarsh Sinha, Peter Hedman, Jonathan T. Barron, Sofien Bouaziz, Dan B Goldman, Ricardo Martin-Brualla, and Steven M. Seitz. Hypernerf: A higher-dimensional representation for topologically varying neural radiance fields. *ACM Trans. Graph.*, 40(6), dec 2021. 2
- [31] Albert Pumarola, Enric Corona, Gerard Pons-Moll, and Francesc Moreno-Noguer. D-nerf: Neural radiance fields for dynamic scenes. In *IEEE/CVF Conference on Computer Vision and Pattern Recognition (CVPR)*, pages 10318–10327, 2021. 2
- [32] Ali Punjani and David J Fleet. 3d flexible refinement: Structure and motion of flexible proteins from cryo-em. *BioRxiv*, pages 2021–04, 2021. 2, 4
- [33] Ali Punjani, John L Rubinstein, David J Fleet, and Marcus A Brubaker. cryosparc: algorithms for rapid unsupervised cryo-em structure determination. *Nature methods*, 14(3):290–296, 2017. 1, 2, 7, 12
- [34] Jeremy Reizenstein, Roman Shapovalov, Philipp Henzler, Luca Sbordone, Patrick Labatut, and David Novotny. Common objects in 3d: Large-scale learning and evaluation of real-life 3d category reconstruction. In *IEEE/CVF International Conference on Computer Vision (ICCV)*, pages 10901–10911, 2021. 3
- [35] Jean-Paul Renaud, Ashwin Chari, Claudio Ciferri, Wenti Liu, Hervé-William Rémy, Holger Stark, and Christian Wiesmann. Cryo-em in drug discovery: achievements, limitations and prospects. *Nature reviews Drug discovery*, 17(7):471–492, 2018. 1, 12
- [36] Alexis Rohou and Nikolaus Grigorieff. Ctfnd4: Fast and accurate defocus estimation from electron micrographs. *Journal of structural biology*, 192(2):216–221, 2015. 5
- [37] Sjors HW Scheres. Maximum-likelihood methods in cryo-em. part ii: application to experimental data. *Methods in enzymology*, 482:295, 2010. 2
- [38] Sjors HW Scheres. Relion: implementation of a bayesian approach to cryo-em structure determination. *Journal of structural biology*, 180(3):519–530, 2012. 1, 2
- [39] Shayan Shekarforoush, David B Lindell, David J Fleet, and Marcus A Brubaker. Residual multiplicative filter networks for multiscale reconstruction. In *Advances in Neural Information Processing Systems (NeurIPS)*, 2022. 2, 12, 14
- [40] Amit Singer and Fred J Sigworth. Computational methods for single-particle electron cryomicroscopy. *Annual review of biomedical data science*, 3:163–190, 2020. 1
- [41] Robin Strudel, Ricardo Garcia, Ivan Laptev, and Cordelia Schmid. Segmter: Transformer for semantic segmentation. In *IEEE/CVF International Conference on Computer Vision (ICCV)*, pages 7262–7272, 2021. 3
- [42] Guang Tang, Liwei Peng, Philip R Baldwin, Deepinder S Mann, Wen Jiang, Ian Rees, and Steven J Ludtke. Eman2: an extensible image processing suite for electron microscopy. *Journal of structural biology*, 157(1):38–46, 2007. 5
- [43] Ashish Vaswani, Noam Shazeer, Niki Parmar, Jakob Uszkoreit, Llion Jones, Aidan N Gomez, Łukasz Kaiser, and Illia Polosukhin. Attention is all you need. *Advances in Neural Information Processing Systems (NeurIPS)*, 30, 2017. 3
- [44] Peihao Wang, Xuxi Chen, Tianlong Chen, Subhashini Venugopalan, Zhangyang Wang, et al. Is attention all nerf needs? *International Conference on Learning Representations (ICLR)*, 2022. 3
- [45] Peng Wang, Lingjie Liu, Yuan Liu, Christian Theobalt, Taku Komura, and Wenping Wang. Neus: Learning neural implicit surfaces by volume rendering for multi-view reconstruction. *Advances in Neural Information Processing Systems (NeurIPS)*, 2021. 2
- [46] Qianqian Wang, Zhicheng Wang, Kyle Genova, Pratul P Srinivasan, Howard Zhou, Jonathan T Barron, Ricardo Martin-Brualla, Noah Snavely, and Thomas Funkhouser. Ibrnet: Learning multi-view image-based rendering. In *IEEE/CVF Conference on Computer Vision and Pattern Recognition (CVPR)*, pages 4690–4699, 2021. 3
- [47] Enze Xie, Wenhai Wang, Zhiding Yu, Anima Anandkumar, Jose M Alvarez, and Ping Luo. Segformer: Simple and efficient design for semantic segmentation with transformers. *Advances in Neural Information Processing Systems (NeurIPS)*, 34:12077–12090, 2021. 3
- [48] Jiakai Zhang, Xinhang Liu, Xinyi Ye, Fuqiang Zhao, Yanshun Zhang, Minye Wu, Yingliang Zhang, Lan Xu, and Jingyi Yu. Editable free-viewpoint video using a layered neural representation. *ACM Transactions on Graphics (TOG)*, 40(4):1–18, 2021. 2
- [49] Fuqiang Zhao, Yuheng Jiang, Kaixin Yao, Jiakai Zhang, Liao Wang, Haizhao Dai, Yuhui Zhong, Yingliang Zhang, Minye Wu, Lan Xu, et al. Human performance modeling and rendering via neural animated mesh. *ACM Transactions on Graphics (SIGGRAPH ASIA)*, 41(6):1–17, 2022. 2
- [50] Sixiao Zheng, Jiachen Lu, Hengshuang Zhao, Xiatian Zhu, Zekun Luo, Yabiao Wang, Yanwei Fu, Jianfeng Feng, Tao Xiang, Philip HS Torr, et al. Rethinking semantic segmentation from a sequence-to-sequence perspective with transformers. In *IEEE/CVF Conference on Computer Vision and Pattern Recognition (CVPR)*, pages 6881–6890, 2021. 3

- [51] Ellen D Zhong, Tristan Bepler, Bonnie Berger, and Joseph H Davis. Cryodrgn: reconstruction of heterogeneous cryo-EM structures using neural networks. *Nature Methods*, 18(2):176–185, 2021. [2](#), [4](#), [6](#), [7](#), [8](#), [12](#)
- [52] Ellen D Zhong, Tristan Bepler, Joseph H Davis, and Bonnie Berger. Reconstructing continuous distributions of 3d protein structure from cryo-em images. In *International Conference on Learning Representations (ICLR)*, 2020. [2](#), [4](#)
- [53] Ellen D Zhong, Adam Lerer, Joseph H Davis, and Bonnie Berger. CryoDRGN2: Ab initio neural reconstruction of 3D protein structures from real cryo-EM images. In *IEEE/CVF International Conference on Computer Vision (ICCV)*, 2021. [2](#), [4](#), [8](#), [14](#)
- [54] Luowei Zhou, Yingbo Zhou, Jason J Corso, Richard Socher, and Caiming Xiong. End-to-end dense video captioning with masked transformer. In *IEEE/CVF Conference on Computer Vision and Pattern Recognition (CVPR)*, pages 8739–8748, 2018. [3](#)
- [55] Yi Zhou, Connelly Barnes, Jingwan Lu, Jimei Yang, and Hao Li. On the continuity of rotation representations in neural networks. In *IEEE/CVF Conference on Computer Vision and Pattern Recognition (CVPR)*, pages 5745–5753, 2019. [4](#)

A. Video

For better visualization of cryo-EM reconstruction results, we use ChimeraX [12] to create a set of video visualizations where reconstructions are rotated, and multiple reconstructed states are played in series. Please check the file *supplementary_video.mp4*.

B. Cryo-EM

Cryo-EM is a revolutionary imaging technique used to discover the 3D structure of macromolecules, including proteins and viruses. It enables structural biologists to understand how these miniature biological machines behave [19, 28, 35]. In a typical cryo-EM experiment, a purified sample containing many instances of the specimen is obtained. This sample is plunged into a cryogenic liquid, such as liquid ethane, which causes the molecules to freeze within a vitreous ice matrix. Once frozen, the sample is loaded into a transmission electron microscope and exposed to parallel electron beams (Fig. 9 (a)), leading to the acquisition of two-dimensional projection images of the Coulomb scattering potential of the molecules (Fig. 9 (b)). These raw micrographs are then processed by algorithms to reconstruct the volume. Cryo-EM reconstruction is a challenging task due to several factors. Firstly, in the micrographs, the poses of the individual particles are unknown, and articles can also adopt multiple conformational states. Secondly, micrographs are acquired under low-dose conditions to limit damage to the radiation-sensitive particles, resulting in low signal-to-noise ratios (typically less than 0.1).

In the cryo-EM image formation model, the 3D biological structure is represented as a function $\sigma : \mathbb{R}^3 \mapsto \mathbb{R}^+$, which expresses the Coulomb potential induced by the atoms. The probing electron beam interacts with the electrostatic potential, and ideally, one can formulate its clean projections without any corruption as

$$\mathbf{I}_{\text{clean}}(x, y) = \int_{\mathbb{R}} \sigma(\mathbf{R}^\top \mathbf{x} + \mathbf{t}) dz, \quad \mathbf{x} = (x, y, z)^\top, \quad (6)$$

where $\mathbf{R} \in SO(3)$ is an orientation representing the 3D rotation of the molecule and $\mathbf{t} = (t_x, t_y, 0)^\top$ is an in-plane translation corresponding to an offset between the center of projected particles and center of the image. The projection is, by convention, assumed to be along the z -direction after rotation. In practice, images are intentionally captured under defocus in order to improve the contrast, which is modeled by convolving the clean images with a point spread function (PSF) g . All sources of noise are modeled with an additional term ϵ and are usually assumed to be Gaussian white noise. The image formation model considering PSF and noise is expressed as

$$\mathbf{I} = g \star \mathbf{I}_{\text{clean}} + \epsilon. \quad (7)$$

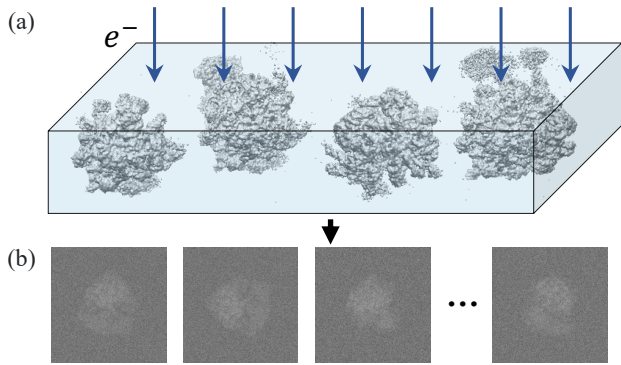


Figure 9. **Illustration of a cryo-EM experiment.** (a) A sample containing molecules of interest is frozen in a thin layer of vitreous ice and exposed to parallel electron beams. (b) Two-dimensional projection images of the Coulomb scattering potential of the molecules. For clarity, we present simulated images with a signal-to-noise ratio (SNR) of 0.1. Note that actual experimental data may suffer from more severe noise.

C. Baseline Settings

CryoDRGN [51]. All cryoDRGN experiments mentioned in this paper were run with its official repository on Github[†].

The setup is that the latent dimension is 8, and both the encoder and decoder are MLPs with 3 layers and 1024 units per layer.

Sparse Fourier Backpropagation [18]. As there is no open-source code available for SFBP, we re-implement the method. We followed the same setting as in the original paper, with an encoder consisting of five layers and a decoder consisting of a single linear layer, 256 units per layer. The number of structural bases used was 16.

CryoSPARC [33]. We follow the software’s defaults for all the settings.

ResMFN [39]. We use the official repository on Github^{*}. We follow the setting of using a 3-layer network with 128 hidden units to represent the 3D structure. The network outputs the structure in 3 hierarchical scales, and the training process is divided into 3 stages, one for each scale. We spend respectively 25, 25, and 50 epochs optimizing the first to the third scales.

D. Additional Results

In this section, we provide additional experimental details and results as a complement to Sec. 5.

Heterogeneous reconstruction of PEDV spike protein. We provide further analysis of the heterogeneous recon-

[†] The repository is available at <https://github.com/zhongge/cryodrgn>.

^{*} The repository is available at <https://github.com/shekshaa/ResidualMFN>.

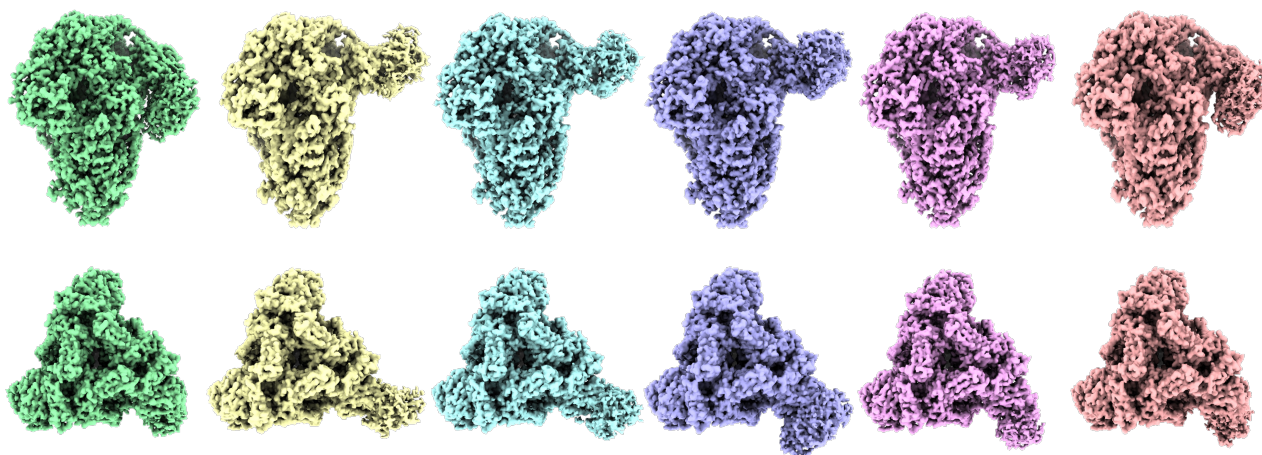


Figure 10. **Our reconstructed states of PEDV spike protein.** We sample six cluster centers in Fig. 11 and visualize the corresponding reconstructed states. The volumes, from left to right, correspond to the following clusters: 5, 6, 4, 2, 8, and 1.

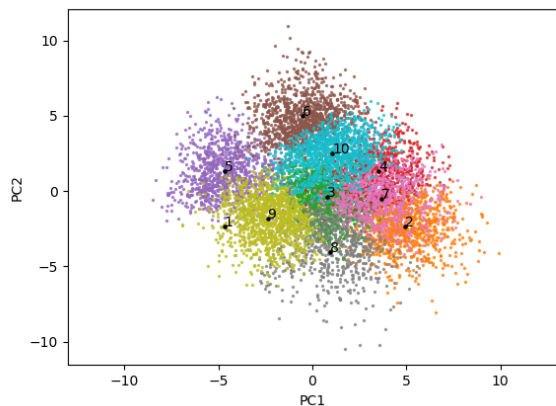


Figure 11. **Distribution of image deformation features.** We visualize the distribution of all the images’ deformation features in 2D with PCA and color-code the points by their corresponding K-means labels. The cluster centers are annotated.

struction performance of cryoFormer on PEDV spike protein dataset. To verify the effectiveness of the deformation encoder, we perform principal component analysis (PCA) on the deformation features of all images and plot their distributions in Fig. 11. We apply K-means algorithm with 10 clusters and color-code the points with their corresponding K-means labels. We display the reconstructed volumes corresponding to 6 of the cluster centers in Fig. 10.

To demonstrate the ability of different methods to handle conformational heterogeneity as well as their reconstruction performance in data, we qualitatively compared their

reconstructions by showing the composition of multiple reconstructed conformations with $\text{SNR} = 0.1$. In Fig. 12, each reconstructed conformation is represented by a different color. It can be observed that our results contain the correspondences of all the states in the ground truth as well as the fine-grained details while the results of cryoDRGN and SFBP have lower spatial resolutions and thus poorer conformation correspondences to ground truth.

Quantitative comparison on EMPIAR-10028. We quantitatively compare different approaches for cryo-EM reconstruction on the real experimental dataset EMPIAR-10028 by the typical practice of splitting the full dataset into two halves, reconstructing each half separately, and computing the FSC between them. We display the FSC curves in Fig. 13. CryoSPARC has the highest half-map FSC curve among the three methods.

Multi-state qualitative comparison on EMPIAR-10076. We provide a more comprehensive multi-state qualitative comparison on EMPIAR-10076 in Fig. 14. We select three states from the reconstructions obtained by different methods and observe them from two views. For ours and CryoDRGN’s results, we can always find three states while ours has more details. For cryoSPARC’s results, we could not find state 2 and it lacks details.

E. Reconstruction without Accurate Pre-computed Poses

Pose refinement serves as a core step for preserving high-frequency details of reconstruction results though jointly estimating accurate poses and reconstructing 3D structures are chicken-egg problems, especially for heterogeneous recon-

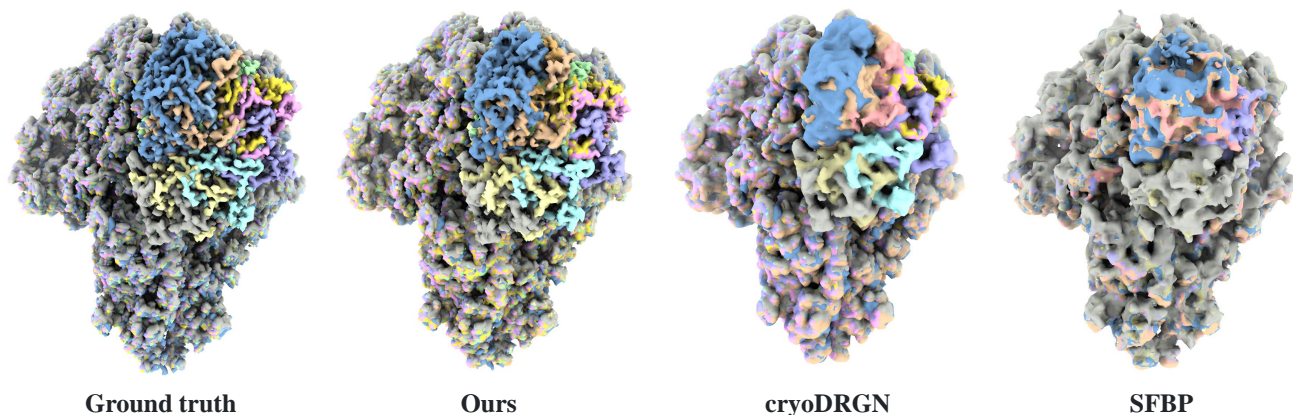


Figure 12. **Different conformational states of reconstruction.** Our method’s reconstruction contains all the corresponding states present in the ground truth while maintaining the details. On the other hand, the reconstructions of the baselines are difficult to differentiate between different states and exhibit inferior details.

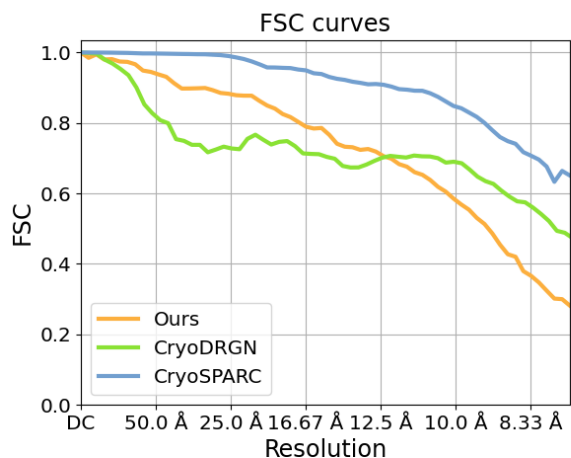


Figure 13. **Quantitative comparison of different methods for reconstruction on real experimental datasets.** The FSC curves are computed between the reconstructions from two halves of the input. A higher curve means a better reconstruction.

struction. Thus, we provide some discussions in this section. For the experiments conducted in Sec. 5 and Sec. D, we assume that accurate poses for all images are known for better expositions, and therefore we directly use the given poses when running our approach and other methods. In this section, we compare our approach with ResMFN [39] for cryo-EM reconstruction in scenarios where accurate pre-computed poses are not available. ResMFN is a multi-scale coordinate network suitable for tasks that involve coarse-to-fine training, and it has been shown to be effective in cryo-EM reconstruction without accurate poses. In line with ResMFN’s experimental setup, we initialize each pose parameter to a random value sampled uniformly from a

geodesic distance of 45 to 90 degrees from the ground truth, which can be considered as a crude initial estimate for poses. To initialize our image orientation encoder, we use all the image-pose pairs to pre-train it until convergence. We then evaluate both methods on the PEDV spike dataset with 20000 images and $\text{SNR} = 0.1$. As shown in Fig. 15, our reconstruction is inferior to ResMFN, which could possibly be attributed to ResMFN’s coarse-to-fine training strategy. Note that this experimental setup differs from ab-initio cryo-EM reconstruction, where no form of information regarding poses is given, including coarse estimates. Our method is not capable of performing ab-initio cryo-EM reconstruction like cryoDRGN2 [53], cryoAI [21] and cryoFIRE [22]. To address this limitation, future improvements may involve incorporating more refined pose estimation modules into our method.

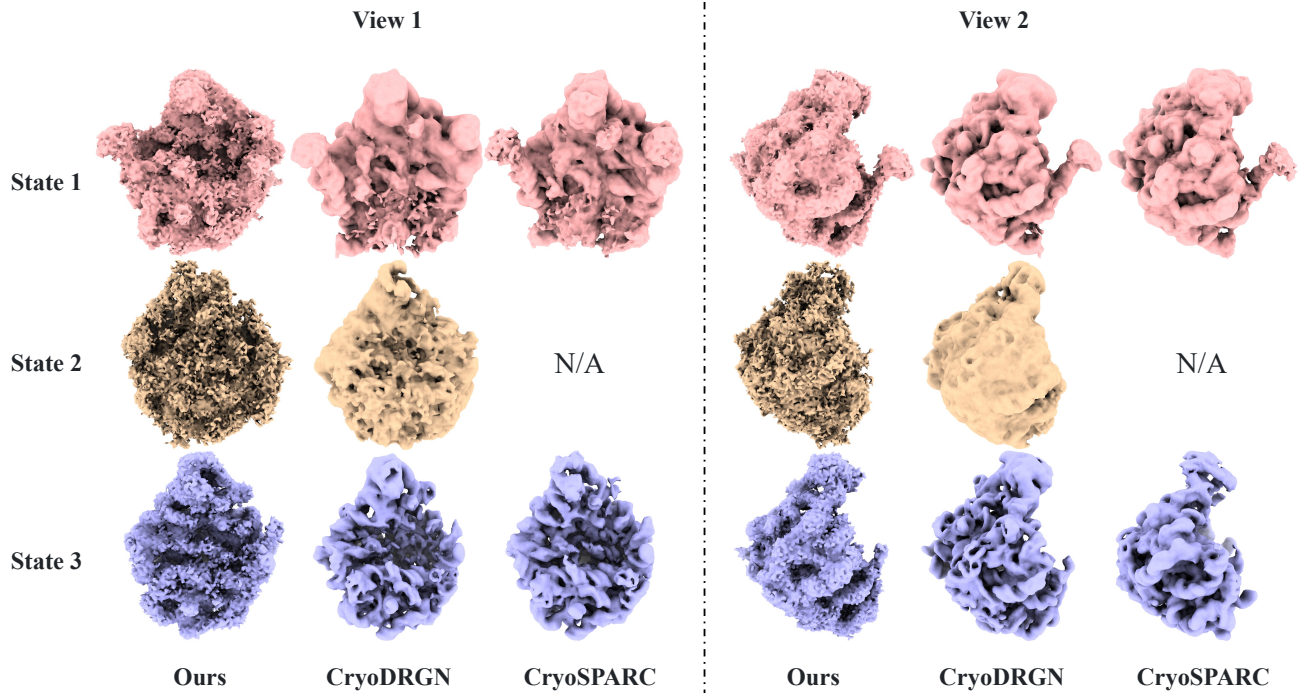


Figure 14. **Qualitative comparison for heterogeneous cryo-EM reconstruction on EMPIAR-10076.** We display three states from the reconstructions obtained by different methods and observe them from two views. Our reconstructions preserve finer details.

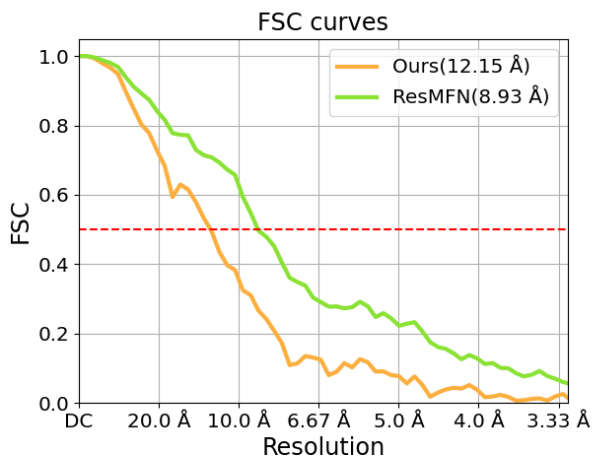


Figure 15. **Quantitative comparison of ours and ResMFN for reconstruction without accurate poses.** FSC curves of cryoFormer and ResMFN for cryo-EM reconstruction without accurate pre-computed poses. A higher curve means better reconstruction.